Structural & electrical characterization of $(Bi_{0.5}Na_{0.5}TiO_3)_{1-x}(BaTiO_3)_x$ solid solution in the vicinity of morphotropic phase boundary

Thesis

Submitted for partial fulfilment for the award of the degree of

MASTER OF SCIENCE (PHYSICS)

THAPAR INSTITUTE
OF ENGINEERING & TECHNOLOGY
(Deemed to be University)

By

Aditi Sharma

(Roll No. 302004002)

Under the supervision of

Dr. Jayant Kolte
Assistant Professor
School of Physics & Materials Science
Thapar Institute of Engineering & Technology, Patiala
Punjab-147004

July 2022

CERTIFICATE

This is to certify that the thesis entitled **'Structural & electrical characterization of $(Bi_{0.5}Na_{0.5}TiO_3)_{1-x}(BaTiO_3)_x$ solid solution in the vicinity of morphotropic phase boundary'** is being submitted by **Aditi Sharma** (Roll no: 302004002) in the fulfilment of the requirement for the award of the degree of Master of Science (Physics) at School of Physics & Materials Science, Thapar Institute of Engineering and Technology, Patiala (Punjab), India. It is an exclusive record of the candidate's own research under me. To the best of my knowledge, this dissertation in part or full has not been submitted in any other institution for the award of any kind of degree.

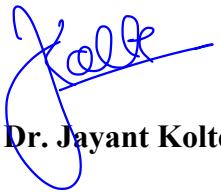

Dr. Jayant Kolte

(Supervisor)

Assistant Professor

School of Physics and Materials Science

Thapar Institute of Engineering and Technology, Patiala

DECLARATION

I hereby declare that the thesis entitled **'Structural & electrical characterization of $(Bi_{0.5}Na_{0.5}TiO_3)_{1-x}(BaTiO_3)_x$ solid solution in the vicinity of morphotropic phase boundary'** submitted to the School of Physics & Materials Science in Thapar Institute of Engineering and Technology, Patiala, is a record of an original work done by me under the guidance Dr. Jayant Kolte, Assistant Professor, School of Physics & Materials Science, Thapar Institute of Engineering and Technology, Patiala.

Aditi Sharma

302004002

Acknowledgement

The pleasure of this note is to thank and express gratitude to all those who have helped me throughout my course since I began my thesis work.

First and foremost, I would like to acknowledge and give my warmest thanks to my supervisor **Dr. Jayant Kolte**, Assistant Professor, School of Physics and Materials Science (SPMS), Thapar Institute of Engineering and Technology (TIET), Patiala (India) for giving me the opportunity to work on such a fascinating topic with all necessary supports and continuous guidance throughout my study. His insightful feedback pushed me to sharpen my thinking and improve my quality of work. As a student, I am grateful to him for providing invaluable, creative and scholarly guidance throughout the course. I am deeply grateful to him for providing invaluable, creative and scholarly guidance throughout the course.

I would like to express my sincere gratitude to **Dr. Kulvir Singh (Head, SPMS)** for his support and guidance throughout the course work. He extended a helping hand to me when I needed it most. I consider myself to be extremely privileged to have been his student.

I would like to thank DST FIST-II for providing the necessary characterization facility like XRD, Raman, and FEG-SEM in School of Physics & Materials Science at Thapar Institute of Engineering and Technology (TIET), Patiala (India).

A special thanks to my senior **Mr. Parminder Singh** for the valuable suggestions, invaluable contribution, moral support, and guidance to enhance my working skills. During every difficult time in the research, I got motivation from him to deal with such challenges.

I am thankful to my lab mates **Ms Taran Dhaliwal, Ms Neha Thakur**, and **Mr Raj Ankit Pandey** for their company during my research work.

A happy cheerful and joyful environment created by my friends **Jaskiran Kaur, Jatin Grover and Neeraj** is always memorable. I am deeply indebted to **Jatin Grover** for his intellectual guidance, inspiration, warmth and generosity. He always supported and encouraged me during all the bad moments.

My words are not sufficient to express sincere gratitude to my mother, **Smt. Amita** and Father **Sh. Rajesh Kumar**. They always stood by my side and supported me unconditionally in every way to achieve what I am today. They made many countless sacrifices and efforts for me to achieve heights. It is worthwhile to acknowledge extraordinary contribution of my grandmother **Late Smt. Asha Rani** and my grandfather **Late Sh. Charanjit Lal Khajuria**. They showered their blessing and inspire me for the higher education. I will always remain in debt to them for giving me strength to reach for the stars and chase my dreams.

I am indebted to my lovable younger brother **Mr. Aditya Sharma,** he supported me relentlessly and made my journey joyful, happier and cheerful. He gave me the strength to live my life to the fullest even through difficult times.

Above all, I surrender before **Almighty God** to reveal my deepest sense of gratitude to **Bless** me with this beautiful life endeavors. Thanks to God for everything in my life. The good and the bad. Some were blessings and some were lessons. I feel fortunate to have an opportunity of exploring the graces of nature.

Aditi Sharma

302004002

Table of Contents

List of Figures

Chapter 1

Introduction

Chapter 3

Experimental Procedure

Chapter 5

Result and Discussion

List of Tables

Chapter 2

Literature review

Abstract

The (1–x) $Bi_{0.5}Na_{0.5}TiO_3$-$x$$BaTiO_3$ (x = 0.04, 0.045, 0.05, 0.055, 0.06) solid solution was prepared by sol-gel method followed by conventional sintering at 1000 °C for 1h. X-ray diffraction and Raman spectroscopy were used to characterize the solid solutions, which revealed that a morphotropic phase boundary (MPB) exists between (x = 0.05-006). A dense microstructure of all specimens has been observed by SEM micrographs. Further their dielectric, ferroelectric, and piezoelectric properties have been studied. With the increasing concentration of BT, the dielectric constant increases to 1155 for x = 0.055 and further decreases. The P-E loop indicates the comparable remnant polarization and low coercive field for all ceramics. The ceramic exhibits strong piezoelectric coefficient at MPB, and for x = 0.055 it exhibits highest d_{33} ~ 105pC/N.

Chapter 1
Introduction

1.1 Introduction

Ceramics are the inorganic materials consisting of metallic and nonmetallic components. Their properties rely on the interconnections between these components [1]. In terms of versatility, ceramics are among the most popular. This versatility comes due to its chemical bonds, which are mainly strong ionic and covalent bonds. These bonds determine the properties of ceramic materials, such as their high modulus, hardness, low ductility and poor thermal properties etc. Ceramics are categorized into two types which are traditional and advanced ceramics as given in Fig. 1.1. Traditional ceramics usually involve silicate glasses, cement, refractories and clay items. Traditional ceramics come from natural sources, such as clay, quartz sand [2]. Advanced ceramics are derived from synthetic raw materials that undergo chemical processes to enhance their physical properties. Advanced ceramics are categorized into structural and functional ceramics.

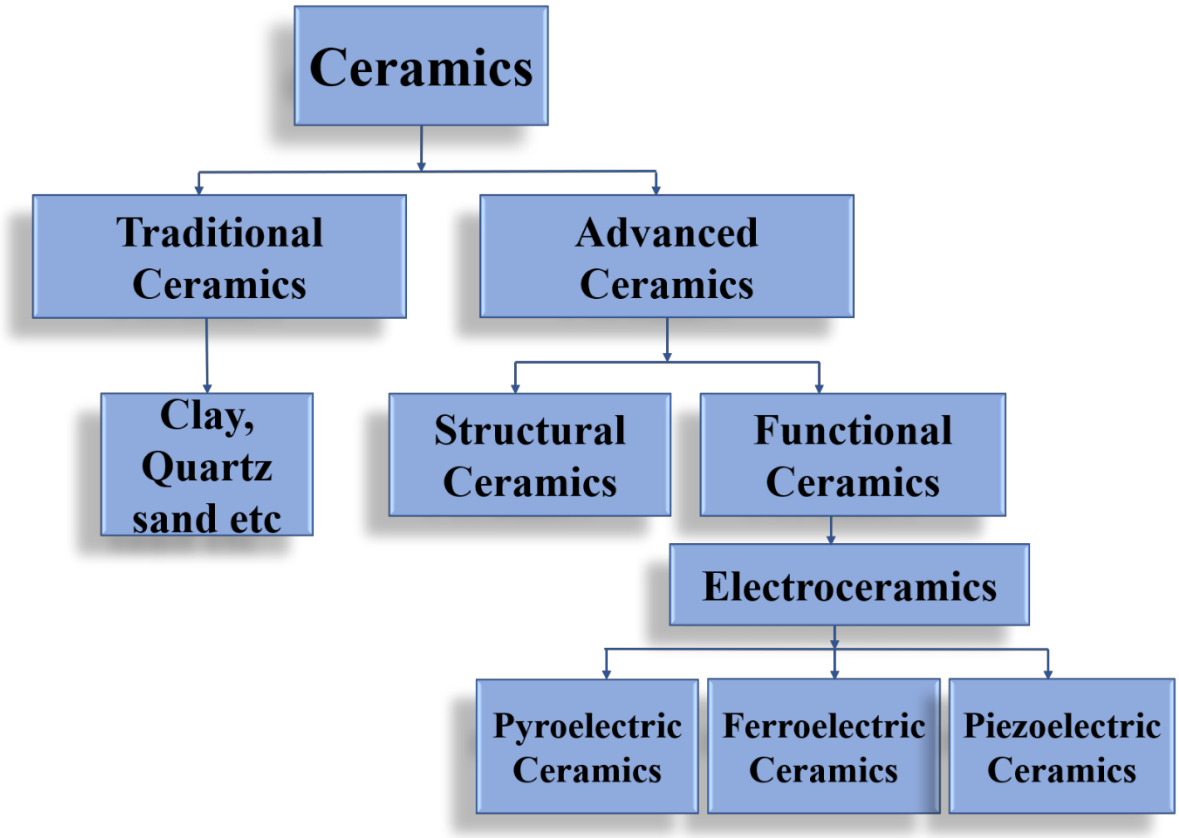

Fig. 1.1 Classification of Ceramics

Structural ceramics are materials which are commonly used for their mechanical characteristics such as excellent strength, hardness, high-temperature resistance, wear resistance that helps to avoid corrosion, bending as well as melting. Functional ceramics are mainly used for their properties such as electrical, magnetic, and optical [3]. Functional ceramic material is usually used in the electronics industry, which is also called electroceramics. Electroceramics are further categorized into pyroelectrics, ferroelectrics and piezoelectrics [4]. Pyroelectric ceramics are commonly used in IR detectors whereas piezoelectric ceramics have many applications in actuators, sensors, sonar etc [5], [6].

Ceramics are well known for their insulating properties, and some ceramics can be converted into excellent dielectrics as well. Mostly ceramics are used in the manufacturing of capacitors. Many studies on the topic of dielectrics are being conducted to enhance their usage in a wide range of fields such as sensors and circuit devices. Ferroelectrics are materials that exhibit spontaneous polarization. The spontaneous polarization generally occurs in highly resistive non-centrosymmetric crystals. Furthermore, such ceramics exhibit good dielectric constant, minimal dielectric loss, and good piezoelectric response [7]. These characteristics are described in detail as follows:

1.2 Dielectrics:

The dielectrics are such ceramics that exhibit spontaneous electrical polarization in an applied electric field. [8].

Faraday was the first scientist who investigates the capacitance of dielectric material. He suggested the capacitance depends on the dielectric material placed in two parallel conducting plates. This study revolutionized insulating dielectric materials for their good charge (q) storage capability [9]. This ability of charge storage is termed capacitance (C) and given as [8].

$$C = \frac{q}{V} = \frac{A\varepsilon}{d} \quad (1)$$

Units of capacitance are Farad.

Where V stands for applied voltage, A is an area, d refers to thickness of dielectric material and ε medium's permittivity.

Further, the extent of data storage in dielectric materials is defined as the dielectric constant. It is the ratio of the capacitance with a dielectric medium between the capacitor plates to the capacitance with a vacuum between the capacitor plates where, $\varepsilon_\circ$ is vacumm's permittivity. It is denoted by ε_r and the formula is given by:

$$\varepsilon_r = \frac{\varepsilon}{\varepsilon_\circ} = \frac{C}{C_o} \quad (2)$$

1.3 Polarization:

Whenever an electric field is applied to dielectrics, positive charges start moving in the opposite direction, while negative charges move in the direction in which the field is applied. This leads to the creation of dipoles; each dipole has a certain dipole moment in the direction of an electric field known as polarization. In other words, it is a dipole moment per unit volume.

$$P = \frac{\mu}{V} \quad (3)$$

There are four types of polarization based on different charge carriers

a) Electronic polarization
b) Ionic polarization
c) Dipolar polarization
d) Space charge polarization

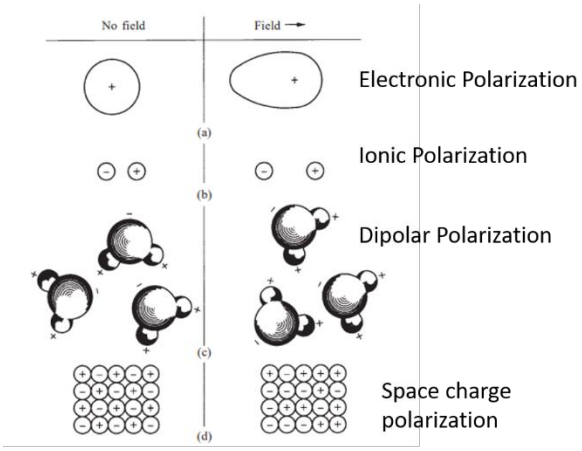

Fig. 1.1 a) Electronic polarization, b) ionic polarization, c) dipolar polarization, d) space charge polarization [10].

1.3.1 Electronic Polarization

This kind of polarization takes place due to the displacement of the negative and positive charge electrons of an atom in the reverse direction when it is subjected to an electric field. The electron cloud around the nucleus moves to the field's positive end. Each atom has a dipole moment because the nucleus and electron cloud are separated. Electronic polarization creates polarization and dielectric constant at optical frequencies.

1.3.2 Ionic Polarization

Ionic polarization arises only in ionic material. On application of an electric field, negative and positive ions displace to their different polarities and form an electric dipole in a solid while in absence of applied field, ions are not displacing from their respective positions. This type of polarization happens in ionic solids like NaCl, KCl, NaF, etc., depending on the crystal structure.

1.3.3 Dipolar Polarization

The polar molecule, which has a permanent dipole moment is subjected to an electric field, the dipoles face torque. As a result, they orient parallel and align in the applied field. This kind of polarization is also known as Orientation polarization and it is temperature-dependent.

1.3.4 Space Charge Polarization

This sort of polarization occurs due to interface/contact electrode charges known as space charge polarization or interfacial polarization.

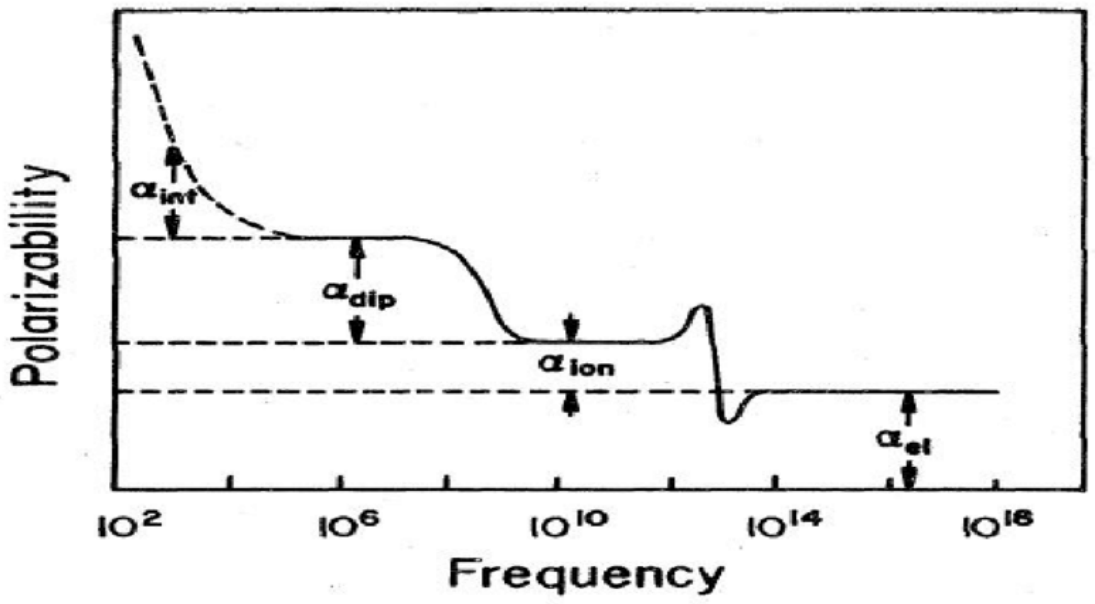

Fig. 1.2 Frequency dependence of polarization processes[10].

1). The process of electronic polarization is very fast. It has a frequency in the optical range (~10^{15} Hz), which is very high.

2). Ionic polarization arises in the infra-red frequency region (~10^{13} Hz) and it is slower than electronic polarization.

3). Dipolar polarization is slower than ionic polarization and mainly occurs in electrical frequency (10^6 Hz).

4). At power frequencies (10^2 Hz), space charge polarization occurs at the slowest rate.

Consequently, at lower frequencies (lower optical frequencies), the total polarization is very high, while at higher frequencies (optical frequencies), the total polarization is very low.

1.4 Ferroelectricity

In 1920, Joseph Valasek revealed that Rochelle salt has permanent polarization in its natural state. Also, he presented the first photograph of the ferroelectric hysteresis cycle [11].

Ferroelectrics are dielectric materials that exhibit a field-controlled hysteresis polarization loop. This ferroelectric behaviour sustains a certain temperature limit and vanishes afterwards. This anomalous behaviour corresponds to Curie temperature (T_c).

Further, these materials exhibit non-zero polarization (say remanence polarization) in the absence of an electric field. Such property causes piezoelectricity in these systems. The cause of field-controlled polarization is domains and domains wall motion. These domains start

responding after the coercive field (E_c) and tend to align themselves in the direction of the applied field. At a certain field, all domains are drifted in the direction of the electric field. At this stage, ceramics exhibits maximum polarization called as saturation polarization[12].

1.5 Properties of ferroelectrics

1.5.1 Crystal Symmetry

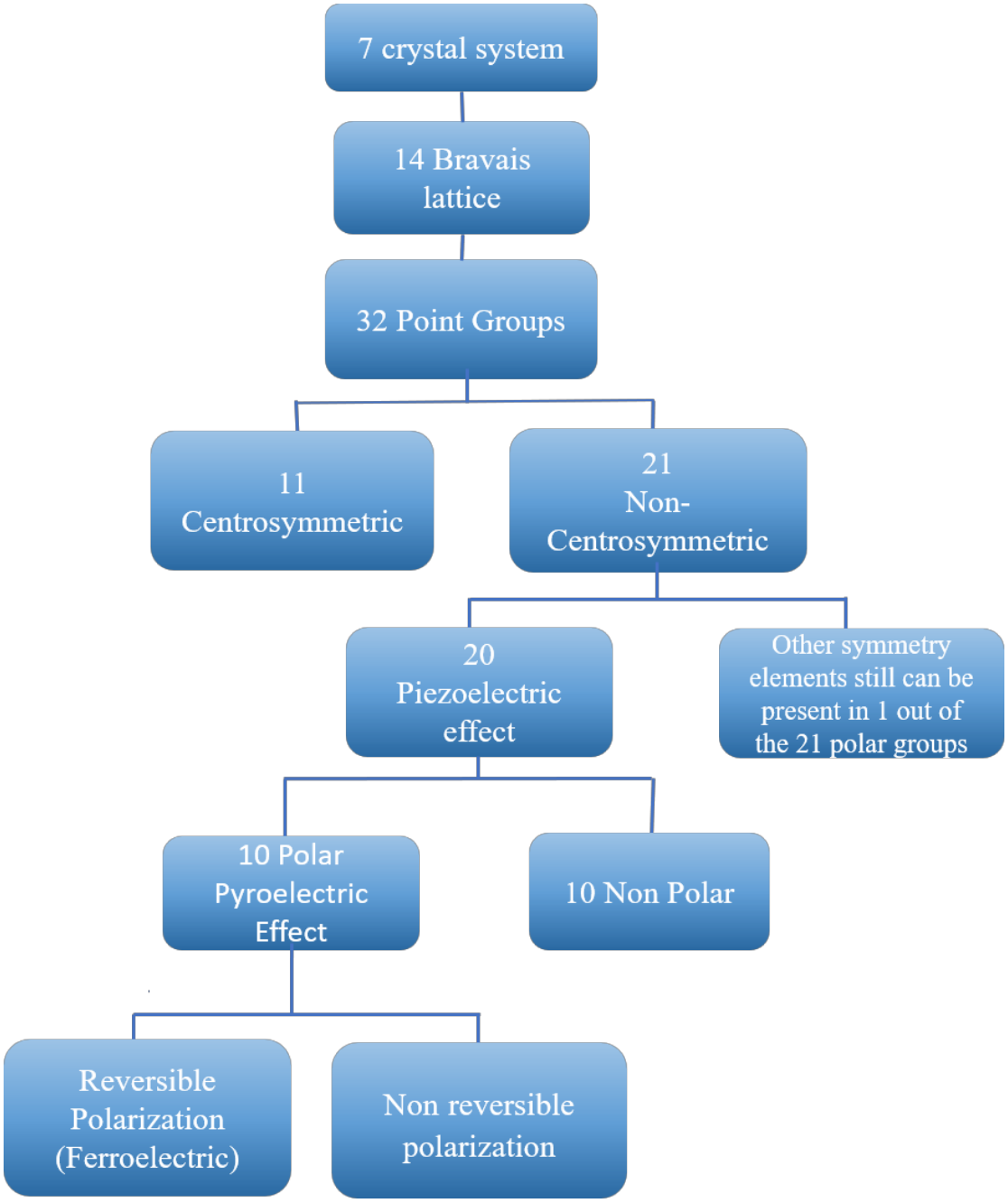

Fig. 1.3 Classification of crystals belonging to the seven lattice systems.

Atoms and molecules are arranged in crystal structures. Crystals are characterized according to symmetry. The seven-crystal system is divided into 14 Bravais lattices, these lattices are further divided into 32-point groups. 32-point groups were subdivided into 11-centrosymmetric and 21 non-centrosymmetric. 11 centrosymmetric relates to non-polar. Out of 21 non-centrosymmetric, 20 exhibit piezoelectricity[12] Fig. 1.4 represents classification of crystals based on their lattice systems.

1.5.2 Pyroelectric effect

In the absence of an electric field, ferroelectric materials possess polarization known as spontaneous polarization and it is temperature-dependent. The pyroelectric effect arises when spontaneous polarization takes place due to temperature change [13]. The temperature change will change the spontaneous polarization if it pre-exists. The polarization of material changes as the locations of atoms alters due to temperature change which gives rise to electric polarization. Pyroelectric polarization will vanish if the temperature remains constant due to leakage current [14], [15].

1.5.3 P-E Hysteresis loop

The ferroelectric behaviour is shown by a crystal when the magnitude and direction of the spontaneous polarization vector P_s are reversed with the application of an external electric field. All the ferroelectrics show pyroelectricity (however a pyroelectric material tourmaline does not show ferroelectricity) but the converse is not true. The nature of the orientation of dipoles in the existence or absence of an external electric field is demonstrated by the ferroelectric domains, which are separated by domain walls.

The direction of P_s can be reversed in ferroelectric materials (shown in the hysteresis loop), which is not true for pyroelectrics. When the electric field increases, the polarization also increases as a result of the alignment of the domains in the direction of the applied electric field. The polarization is limited by a saturation value at a higher value of the electric field. However, when the external field is removed, the polarization doesn't eventually drop to zero, rather attains a remanent polarization value P_r. An oppositely directed electric field, resulting in complete depolarization, is called coercive field strength E_c. Fig. 1.4 illustrates the P-E hysteresis loop for the ferroelectric crystal.

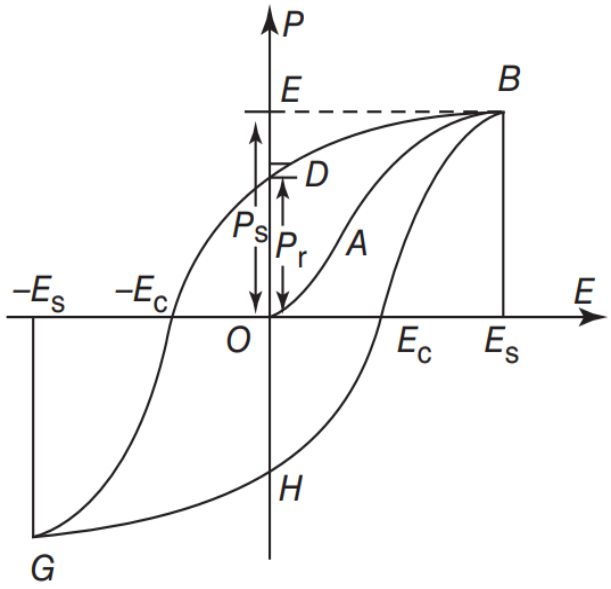

Fig. 1.5 PE hysteresis loop for the ferroelectric crystal[16].

1.6 Piezoelectricity

The phenomenon of energy conversion from mechanical (vibration) to electrical signal is known as piezoelectricity. In eighteen century, Charles Augustin de coulomb was the first to suggest that some solids might show an electrical response if placed under mechanical stress. In 1880, Nobel laureates Pierre and Jacques Curie demonstrated the piezoelectric effect. Piezoelectricity relates to the capability of certain materials, most notably ceramics, to generate an electrical potential when subjected to mechanical stress. There are two types of piezoelectric effects as follows: -

a) Direct Piezoelectric effect
b) Inverse Piezoelectric effect

Direct Piezoelectric effect is, when a compressive or tensile force is applied, a potential difference is produced in the material, while the Inverse Piezoelectric effect takes place when an electric field is introduced to a piezoelectric material, resulting in mechanical stress as shown in Fig. 1.6.

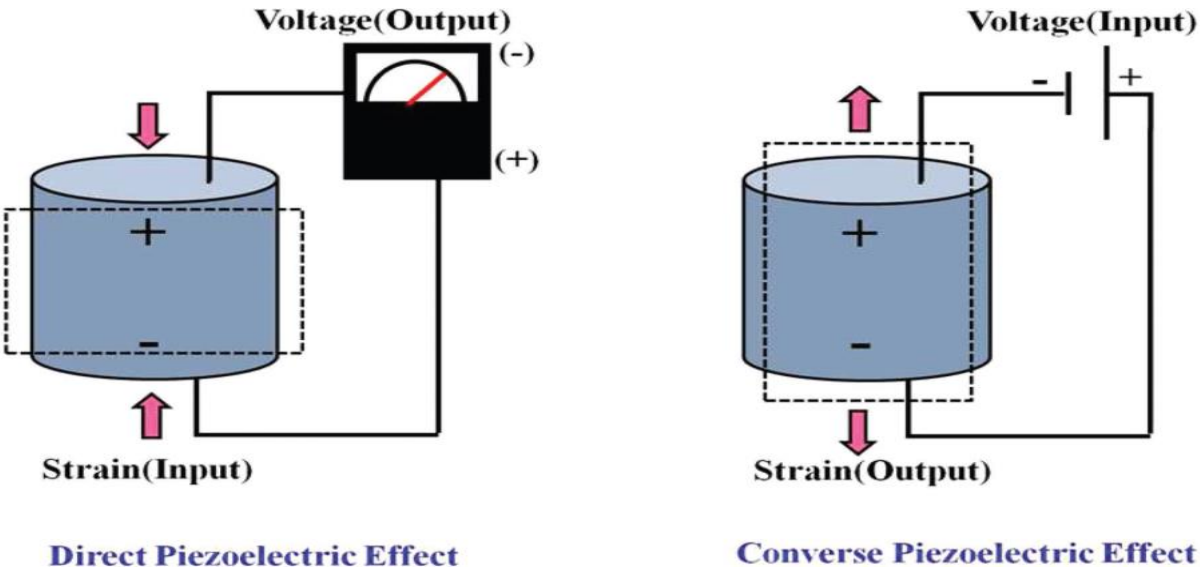

Fig. 1.6 Illustration of piezoelectric effect[17].

During the first World War, the very first practical application of piezoelectricity was the discovery of sonar. Paul Langevin and his co-workers employed piezoelectric transducers to overcome the issues of submarine detection. The piezoelectric effect was firstly observed in naturally produced crystals like quartz and tourmaline. For piezoelectric devices, quartz was primarily used before the invention of man-made crystals[18]. During the Second World War, several research groups in Russia, US and Japan created piezoelectric materials with outstanding piezoelectric properties than naturally existing materials. In the 1950s barium titanate was the first synthetic piezoelectric material which leads to the creation of PZT. This results in a wide range of applications such as enhanced sonar devices, microphones, piezoelectric filters, and buzzers. Piezoelectric devices are now widely used in daily electronics systems such as cellphones, radios, fire alarms, medical devices, microwave ovens etc[19].

The piezoelectric effect can be described by knowing the internal structure of the crystal or solid. The solid consists of atoms and ions arranged in long-range order in a definite repeating pattern, known as crystalline solids. The crystal lattice is a three-dimensional structural setup of ions, atoms and molecules which forms a unit cell. As piezoelectric material consists of multiple unit cells and all of these have randomly scattered dipole moments. When a material is subjected to an electric field or mechanical stress, each dipole alters its orientation. The dipole moment's direction is strongly linked to the piezoelectric phenomenon. A high electric field requires poling to align the dipoles. On applying a high electric field on material typically at curie temperature, almost all the dipoles align in the applied field’s direction. The Fig. 1.7

illustrates a basic model to describe the piezoelectric effect. It is well known that piezoelectric materials are made up of several unit cells. The dipole moments of the unit cells are randomly oriented and distributed. Dipoles can change their orientation during the application of an electric field or mechanical stress.

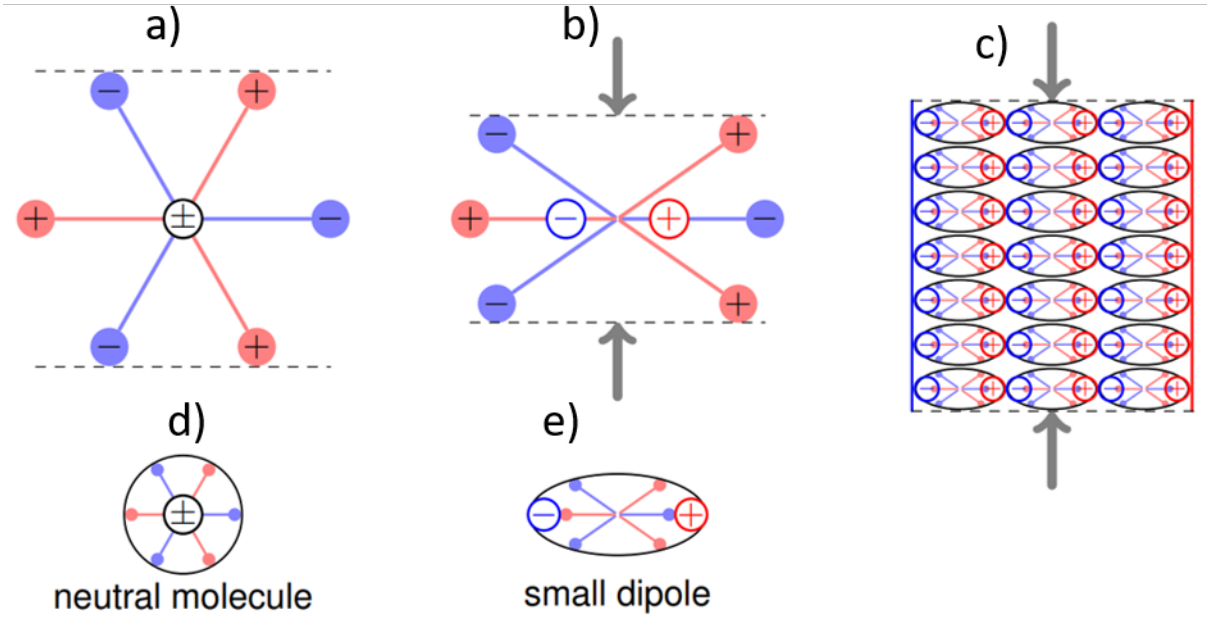

Fig. 1.7 Model to explain the piezoelectric effect[20].

Piezoelectric materials shows amazing electromechanical conversion properties due to which they received a lot of attention in the field of energy harvesting[21]. Piezoelectric materials based on lead zirconate titanate (PZT) are well known for their excellent piezoelectric properties and they are often used in the manufacturing of actuators, sensors and microelectronic devices[22]. Unfortunately, due to high toxicity, the usage of lead-based piezo materials has resulted in huge contamination and environmental issues. With growing environmental concerns about lead-based piezoelectric materials, it is necessary to formulate lead-free piezoelectric alternatives. Over the last two decades, many lead-free piezoceramics have been considered possible alternatives for Pb-based piezoceramics[23].

1.7 Lead-Free Piezoelectric Ceramics

1.7.1 Bismuth Sodium Titanate

Bismuth sodium titanate is regarded as one of the best suitable lead-free piezoelectric materials. Manufacturers demand ceramics which possess a better dielectric constant to make small communication devices. As BNT exhibit a high-temperature dielectric constant it can

give good performance. BNT seems to be a material which will be used in future piezoelectric devices and dielectric materials that work over a large temperature range. Bismuth sodium titanate ceramics possesses a high Curie temperature (~320°C).

At room temperature, BNT behaves like ferroelectrics. It exhibits a perovskite crystal structure with a formula ABO_3 with rhombohedral symmetry[12].

1.7.2 Structure of Bismuth Sodium Titanate

The structure of bismuth sodium titanate (BNT) is similar to the ABO_3 type distorted perovskite having rhombohedral R_3c structure at room temperature. In standard form, BNT is represented as $(Bi_{0.5}Na_{0.5})TiO_3$. An ABO_3 type perovskite structure can be represented in the following way: the sodium (Na^+) and bismuth (Bi^{3+}) cations are located in the corners of the cubic unit cell, the oxygen (O^{2-}) cations occupy the face centres, whereas the Titanium (Ti^{4+}) cation occupies the centre of the oxygen octahedral (as shown in the schematic Fig. 1.8 below)[24].

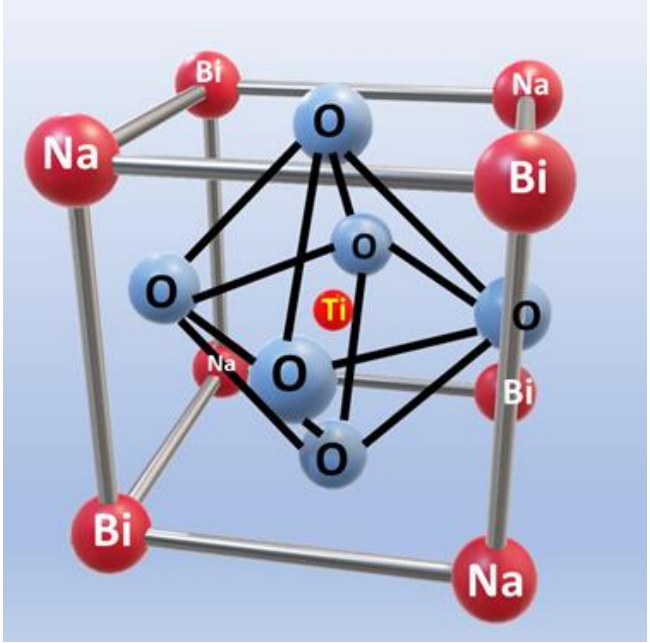

Fig. 1.8 Perovskite structure of sodium bismuth titanate.

1.7.3 Barium Titanate

During the second world war, barium titanate ($BaTiO_3$) was discovered by the US, Russia, and Japan. Due to its outstanding properties, barium titanate has grabbed the attention of scientists. It was the first lead-free piezoelectric material has been used to replace lead-based materials. BTO ($BaTiO_3$) shows excellent ferroelectric properties and a high dielectric constant due to

which it has wide applications in semiconductors, and thermistors and has become the most significant ferroelectric ceramic. Ferroelectric BTO has a curie temperature order ~ 120^0 C and exhibits low dielectric loss. It does not show high piezoelectric constant but exhibits high permittivity which can be used for capacitors[25].

1.8 Perovskite Structure

BTO ($BaTiO_3$) possesses a perovskite structure and has a chemical formula of ABO_3. Generally, the perovskite structure is a 3D framework of BO_6. As in the figure, the basic structure is a primitive cube. It is clear that each barium ion is surrounded by twelve Oxygen ions hence barium and oxygen ions form an FCC lattice. Ba^{2+} ions lie at vertices, Ti^{4+} in body-centred and O^{2-} in face-centred positions in crystal[26].

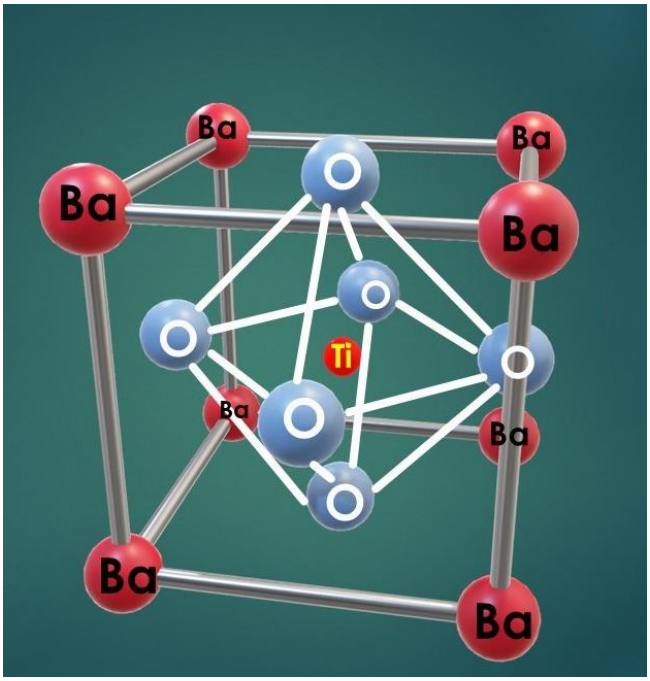

Fig. 1.9 Cubic perovskite-type structure ABO_3.

The Curie temperature of BTO is 120° C. Above this temperature, unit cell is cubic in shape while below the curie point structure starts changing from cubic to tetragonal due to the dipole moment's orientation. Below the 0°C it is orthorhombic, and rhombohedral for temperatures below -90°C. Fig. 8 illustrates unit cells of four phases.

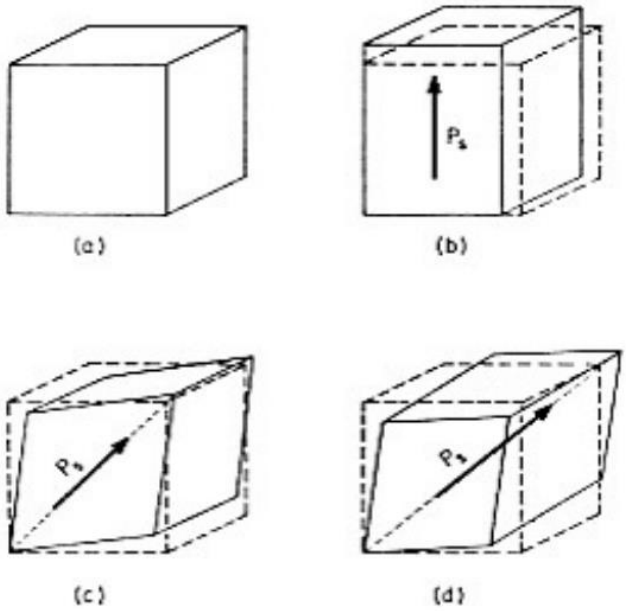

Fig. 1.10 a) Crystal structure of $BaTiO_3$ is cubic at 120°C b) Tetragonal, below the curie point (120°C to 5°C), c) Orthorhombic and stable between 5°C d) Rhombohedral below -90°C [27].

Chapter 2
Literature Review

2.1 Literature Review

The piezoelectric effect was first discovered in 1880 by Pierre Curie and Jaques Curie. The effect was observed on natural crystals, i.e., tourmaline, quartz, and Rochelle salt [28]. Its applications were used first in sonar during the first World War[29]. After its successful implementation, researchers in the US, Russia and Japan developed artificial piezoelectric materials to enhance piezoelectric responses that were superior to naturally occurring materials. Near the second world war, a well-known material barium titanate was first synthesized. Further, the lead zirconate titanate (PZT) piezoceramic was developed in 1950. Its good piezoelectric response was useful to obtain high-performance actuators and transducers. The PZT family has been dominated over other piezoceramics for more than sixty years. Lead-based materials were broadly utilized by industries for shipbuilding, lead-acid battery, and marine applications due to their high d_{33} 130~317 pC/N whereas PMN-PT exhibits a piezoelectric coefficient(d_{33}) ~324-1780 pC/N [30]–[32].

Lead is recognized as a threat to human health due to its adverse effects on mental and neurological development. It is common to experience fatigue, muscle aches, abdominal pain, etc. In lead-based materials, the lead evaporates during the processing of ceramics which cause a serious threat to researchers' mind and pose them to develop its alternate [33]–[35]. There have been various lead-free perovskite materials were investigated likely BT, BKT, BNT, and KNN. Amongst, BNT has been found as a potential candidate due to its good ferroelectric properties, Curie temperature, and piezoelectric response [36]–[40]. BNT possesses large remanent polarization P_r ~ 38 μC/cm^2, high coercive field (Ec) ~ 63 kV/cm and piezoelectric coefficient (d_{33}) of 70-90 pC/N[41], [42]. Due to its high coercive field, BNT is hard to pole. Consequently, BNT is not able to exhibit a high piezoelectric response [43]. So, to reduce its coercive field (E_c) many attempts have been made by researchers and making its solid solution by substituting other piezoelectric ceramics likely BT, KNN, BKT, BMT, ST or doping of some elements (Ce, La, Sr etc) at A and B site of its crystal structure. Several studies on BNT can be performed to determine how doping affects the properties of the material and different

dopants affect the different properties of the material. It has been shown that some studies focus on dielectric properties, while others focus on electrical and piezoelectric properties. In addition of Ce as a dopant in BNT shows a dielectric constant equal to 672 and exhibits low dielectric loss[44][45]. However, the addition of Mn, Nb, and Ba enhances the piezoelectric response of BNT. The doping of Li and Hf enhances the piezoelectric coefficient $d_{33} \sim 100$ pC/N[46]. Table2.1 depicts the piezoelectric coefficient of BNT ceramics with ion substitution.

Table 2.1. Piezoelectric coefficient of BNT ceramics with ion substitution

Composition	d_{33} (pC/N)	References
$Bi_{0.5}Na_{0.5(1-1.5x)}La_xTiO_3$ (x = 1 at.%)	92	[47]
$Bi_{0.5}Na_{0.5}Ti_{1-x}Mn_xO_3$ (x = 0.25%)	105	[48]
$(Bi_{0.5}Na_{0.5})_{1-x/2}(Ti_{1-x}Nb_x)O_3$ (x = 0.02)	87	[49]
$(Bi_{0.96}La_{0.04})0.5(Na_{0.975}Li_{0.025})_{0.5}TiO_3$	70	[50]
$(Bi_{0.5}Na_{0.5-y}Li_y)(Ti_{1-x}Hf_x)O_3$ (x = 0.03, y = 0.01)	100	[46]

The dopants were not able to make a significant contribution towards enhancing the piezo response of BNT as compared to solid solutions. Today the research focus is shifted towards enhancing the piezo response of ceramics by making solid solutions at the morphotropic phase boundary (MPB), where different non-centrosymmetric crystal phases coexist.

BNT-BCT, BNT-BT, BNT-KNN, BNT-BMT, and BNT-BKT solid-solution ceramics are all being worked on by researchers to overcome the poling problem. Among all these, the BNT-BT solid solution has received considerable attention as there is the existence of a rhombohedral (F_α) – tetragonal(F_β) morphotropic phase boundary at x = 0.06 – 0.08, where there is less coercivity and gives better piezoelectric properties[51]–[54]. Table 2.2 depicts the piezoelectric coefficient of various morphotropic BNT solid solutions.

Table 2.2. Piezoelectric coefficient of various morphotropic BNT solid solution

Material System	E_c (kV/cm)	P_r (μC/cm^2)	d_{33} (pC/N)	Ref.
BNT	73	38	98	[55]
BTO	-	-	330	[56]
BKT	52.5	22.2	69.8	[57]
0.965BNT-0.035BT	23	34.8	138	[58]
0.94BNT-0.06BT	27.1	26.3	112	[59]

0.975BNT-0.025BCT	52.5	35.4	107	[60]
0.96BNT-0.04KNN	28	26.96	96	[61]
0.97BNT-0.03BAG	48	28.3	93	[62]
0.9625BNT-0.0375BZT	35	36.5	92	[63]
0.95BNT-0.05BMT	40	18	110	[64]
0.76BNT-0.24ST	20	17	127	[65]
0.96BNT-0.04BAT	20	10	127	[66]
0.955BNT-0.045BNN	17	20	121	[67]

2.2. Literature Gap

The literature review suggested that good piezoelectric response exhibits at MPB. BNT-BT solid solution possesses excellent d_{33} in range of x= (0.04-0.06). However, there is the lack of information about structural, dielectric, ferroelectric and piezoelectric properties in this particular range (x=0.055-0.06). Considering this gap investigation of the structural, dielectric, ferroelectric, and piezoelectric properties in the MPB region has been planned for present work.

2.3. Objectives

Based on the literature survey the following objectives are decided.

1. To make solid solutions of $(1–x)\ Bi_{0.5}Na_{0.5}TiO_3$-$x$$BaTiO_3$ with x = (0.04, 0.045, 0.05, 0.055, 0.06) ceramics by sol-gel method.

2. To study phase, structural and electrical properties of the solid solutions.

Chapter 3

Experimental Procedure

3.1 Experimental Procedure

The solid- solution of BNT-BT has the general formula (1-*x*) $Bi_{0.5}Na_{0.5}TiO_3$- *x*$BaTiO_3$ is synthesised via sol-gel method.

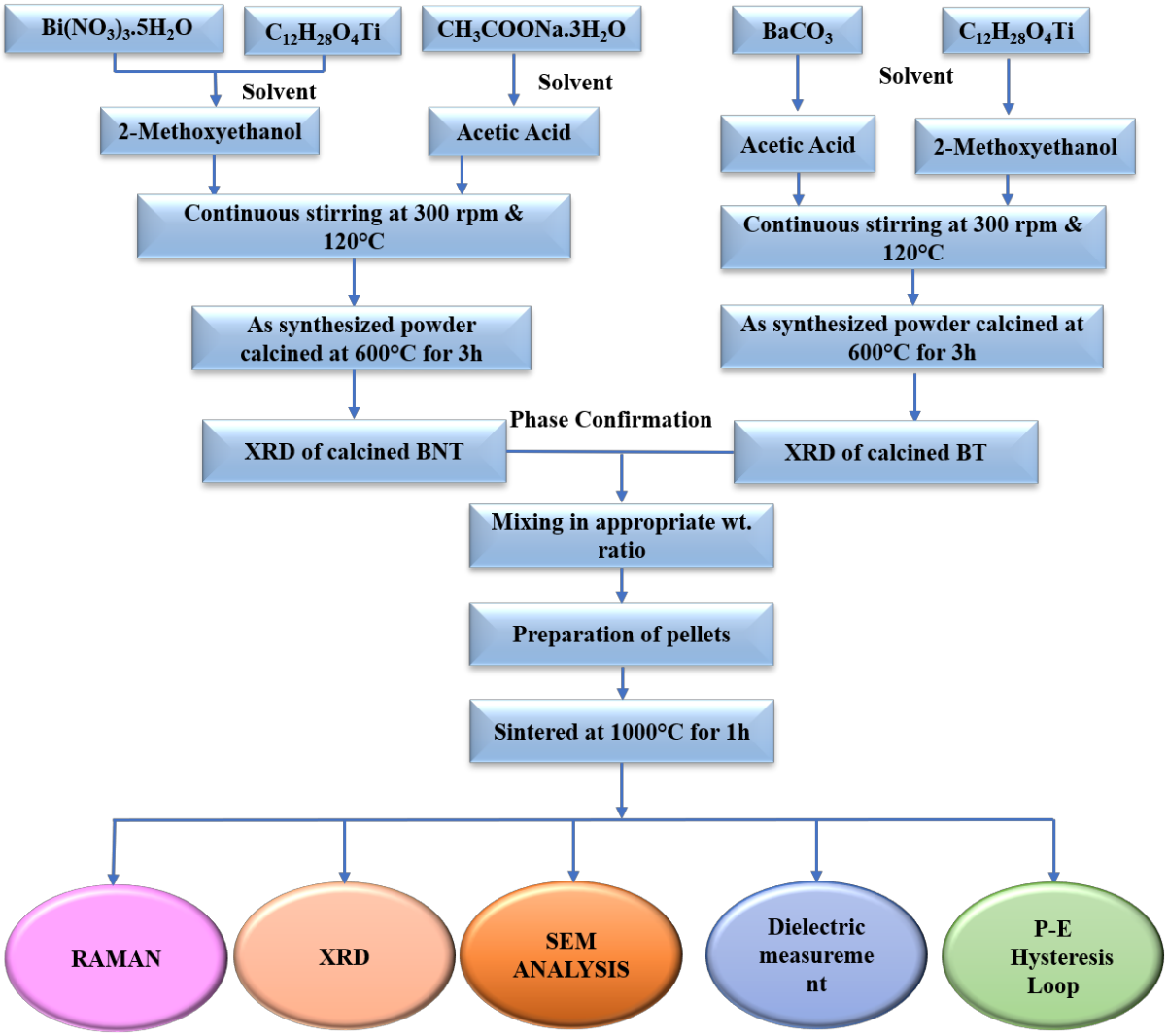

Fig. 3.1 Flowchart for preparation of (1-x) BNT-xBT

Fig. 3.1 The pictorial representation of the synthesis process of BNT-BT. For powder preparation bismuth nitrate pentahydrate ($Bi(NO_3)_3.5H_2O$), titanium isopropoxide ($C_{12}H_{28}O_4Ti$), sodium acetate ($CH_3COONa.\ 3H_2O$), barium carbonate ($BaCO_3$) were taken as

raw material for the synthesis of 2g of BNT-BT. Based on the stoichiometric ratio, the powder was weighed and mixed properly in dry condition. To reduce particle size and homogenous mixing of powder, it was roll milled in the acetonic medium for 6 hours with zirconium balls. Roll milled powder was taken into an alumina crucible and calcined at 600°C for 3 hours to confirm the phase formation. The purpose of calcination is to remove water and volatile substances from a sample by subjecting it to heat below its melting point without fusing. Also, it affects ion interdiffusion among constituents, phase transitions, and electromechanical properties. Then the Poly Vinyl Acetate (PVA) binder was mixed in calcined powder and left to dry. Due to the better mechanical stability, PVA is commonly used as a binder in dry-pressed ceramics. Also, binders can be easily removed from the system during the sintering process. After the addition of PVA, the powder was ground again for 30 minutes to obtain a fine powder. After weighing all the powder compositions, they were packed separately and then pressed into pellets by using a die set with a load of 5 tons. The compacted pellets were placed on an alumina plate and sintered in a conventional furnace at 1000°C for 1 hour. For the pellet to gain more mechanical strength and densification, the sintering process is essential. Atomic diffusion plays a role in the sintering process which causes densification, reduces the porosity between particles and helps in grain growth. Pellets were finely polished with the help of emery paper. The polished pellets were subjected to ultrasonic cleaning for 5 minutes by immersing it in acetone. Further, pellets were coated with silver paste for electroding and left to dry for 60-70°C for 30 minutes. Further, subsequent characterization of the sample were studied.

Chapter 4

Characterization Techniques

4.1 CHARACTERIZATION TECHNIQUES

Various techniques were used to characterize the samples, such as Scanning electron microscope (SEM) X-ray diffraction (XRD), Raman spectroscopy and dielectric measurements.

4.1.1 X-ray diffraction (XRD)

XRD technique has been broadly used to determine the grain size, solution composition, atomic spacing, crystal structure, phase analysis in crystalline substances. In addition to phase identification, X-ray diffraction can also give information regarding the dimensions of unit cells.

Diffraction is entirely determined by constructive interference between monochromatic X-rays and crystalline samples. The X-rays are produced by a cathode ray tube. The electrons which are sufficiently energetic are ejected from the inside shell of the target material, producing characteristic X-ray spectra i.e k_α and k_β. As a result of these X-ray monochromatic radiation is produced. As a target material, copper is commonly used, since its wavelength equals 1.5418 Å for Cu K_α radiation. A beam of X-rays is focused and directed at the provided sample. Each electron scatters radiation in multiple directions after being struck by an x-ray. It is possible to observe constructive interference between X-rays and a sample also satisfies Bragg's law. According to Bragg's law i.e., **$2d\sin\theta = n\lambda$.** Once the sample has been scanned, diffraction patterns are obtained using an angle range of 2θ[68].

In the present study, calcined powders were characterized at room temperature to identify phase, phase quantity and crystallite size etc by using the Rigaku, SmartLab SE with Cu K_α radiation (λ_{inc} =1.54056 Å) having a range 20° to 80°and step size 10 operated at room temperature.

Specifications of used X-ray Diffractometer

Model: Rigaku, SmartLab SE (Japan)

Source: Cu target X−Ray tube 2θ°

Wavelength: 1.54 Å

4.1.2 Scanning Electron Microscope (SEM)

Scanning Electron Microscope (SEM) is an effective tool for studying the surface topography and morphology of materials with high resolution. It is based on the principle that when the beam of electrons produced by the electron gun falls on the specimen then there is an ejection of X-rays, secondary electrons, and backscattered electrons from the given specimen. The detector collects all these electrons and transforms them into a signal which further amplifies and displays on the monitor. Images obtained with SEM exhibit a greater depth of field, creating a 3D appearance that is useful for understanding the surface properties of the sample[69].

In the present study, the JEOL JSM-5300 microscope has been used for the examination of the surface morphology of the sample. Before SEM, silver sputter metal contact was done on the samples of different compositions to make them conduct.

Specifications of used SEM

Model: Carl Zeiss Sigma 500

Sample size < 150 mm

Resolution: 0.8 nm (15 kV)

1.4 nm (1 kV)

Magnification: 10x - 10,00,000x

4.1.3 Ferroelectric measurement

To verify a material's ferroelectric property, hysteresis measurements are carried out. Polarization versus applied field (E) is plotted by a P-E loop tracer at a certain frequency. Through the study of the hysteresis loop, one can determine spontaneous polarization (P_s), remnant polarization (P_r), and coercive fields (E_c).

This study used the Radiant technology PE loop tracer to determine the polarization in different fields. Samples were measured at 2.5 kV.

Specifications of used Hysteresis instrument

Model: Marine India

Thickness < 0.5 mm

Maximum Voltage: 2.5 kV

Frequency: 1 Hz

4.1.4 DIELECTRIC MEASUREMENT

Generally, ferroelectric materials act as the dielectric material. The stability of any ferroelectric material depends on the dielectric properties like the dielectric constant (ε_r) of the material for application purposes.

To measure dielectric constant, the pellets were first coated with a silver paste to make it conducting. Then the LCR meter is used for the measurement at room temperature for different frequencies (From 100 Hz to 1 MHz). The LCR meter was connected to the computer where the data of capacitance and dissipation was collected as a function of frequency. The following formula was used to convert the measured capacitance into a dielectric constant:

$$C = \frac{q}{V} = \frac{A\varepsilon}{d} \quad (4)$$

Where C is the capacitance of the capacitor, q is a charge, V is the potential difference applied between plates, A is an area of plates, d is the distance between the capacitor plates and ε is the permittivity of the medium.

$$\varepsilon_r = \frac{\varepsilon}{\varepsilon_\circ} = \frac{C_d}{C_A} \quad (5)$$

where ε_r is the dielectric constant, $\varepsilon_\circ$ is vacumm's permittivity.

4.1.5 RAMAN SPECTROSCOPY

The Raman Spectroscopy technique provides information regarding chemical structure, phase, crystallinity, and molecular interactions without causing any damage to the sample.

Raman scattering uses a laser to scatter light from a molecule. During this process, light interacts with the chemical bonds in a material. In most cases, the photons scatter from the sample without changing energy, but in some cases, a few photons exchange energy and cause molecules to vibrate which is known as the Raman effect.

In the present study, Labram HR Confocal Micro-Raman Spectrometer equipped with solid state laser is used as an excitation source to obtain spectra in the wavelength of 532 nm and diffraction grating of 1800 lines/mm.

Specifications of used Raman Spectrometer

Model: Labram HR Confocal Micro-Raman Spectrometer

Excitation sources: 325 nm, 532 nm and 785 nm

Grating: 300,600,1800,2400l/mm

Chapter 5

Result and Discussion

5.1 X-ray Diffraction (XRD)

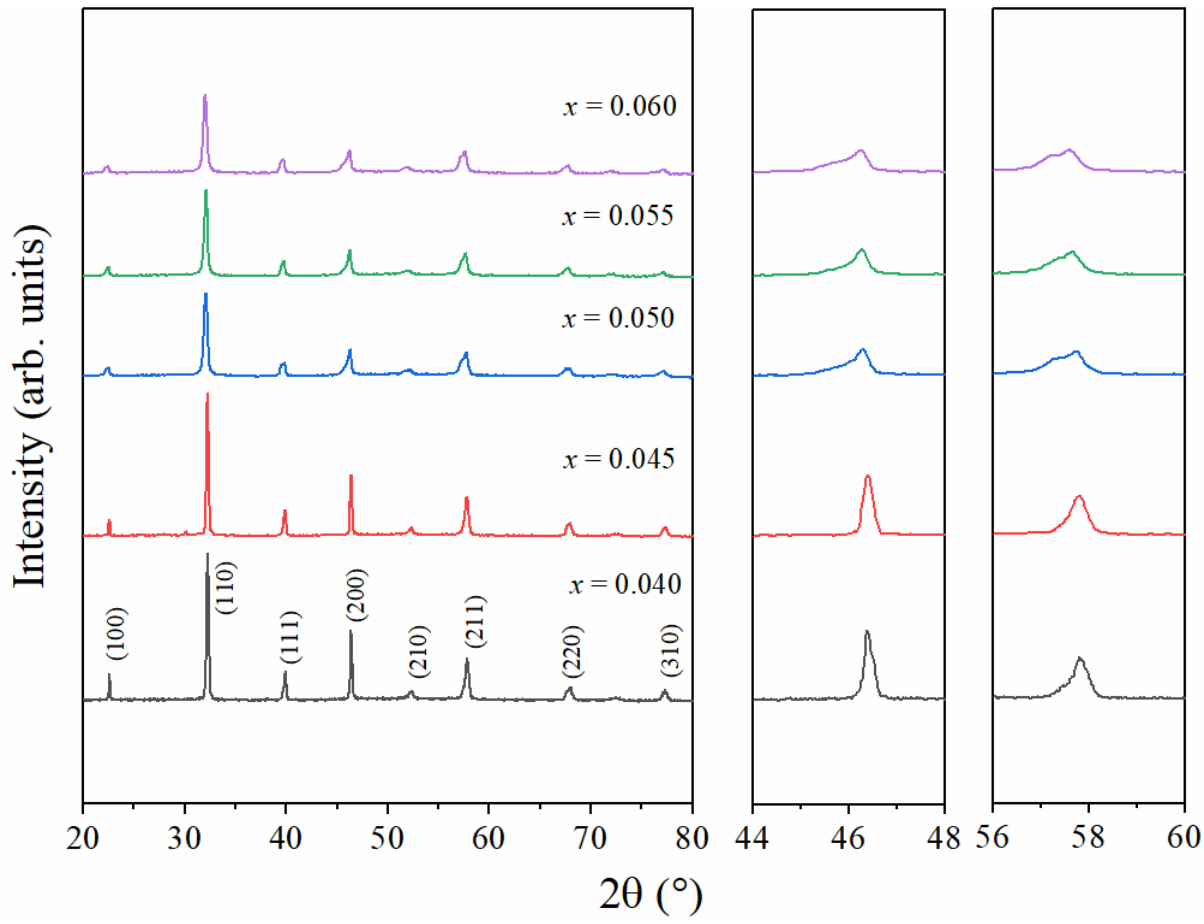

Fig. 5.1 X- Ray diffraction pattern of $(1–x)\ Bi_{0.5}Na_{0.5}TiO_3$-$xBaTiO_3$ with x = (0.04, 0.045, 0.05, 0.055, 0.06).

The XRD pattern helps to obtained the phase and structural information of the ceramics. The XRD pattern of BNT-BT in 2θ ranges 20-80° has been carried out to study the effect of BT content on the phase and structure of BNT-BT solid solution and depicted in Fig. 5.1. It has observed that all intensity peaks are matched with R3c BNT with slight shift with BT composition (see Fig. 5.1 (b)). The slightly higher ionic radii of Ba^{2+} (1.61Å) as compared to Bi^{3+} (1.17Å) as well Na^{+} (0.97Å) preferably occupies A-site of perovskite structure that causes

compressive strain in crystal and shift the peak towards lower angle side in accordance to the Scherrer formula. Scherrer formula is given by:

$$D = \frac{K\,\lambda}{\beta\,cos\theta} \tag{6}$$

Where, K = Scherrer constant = 0.89

λ = wavelength of Cu-K_α

β = full width at half maxima

θ = diffraction angle

The lack of any additional peak has been observed in pattern that confirm the absence of any additional/impure phase [70]–[72]. BNT-BT ceramic displays rhombohedral crystal structure for $x = 0.040$ and 0.045 (as all the peaks are matched with R3c BNT). For $x > 0.045$, the splitting of peak in range 56-60° suggest the coexistence of rhombohedral-tetragonal phases.

5.2 Raman Investigation

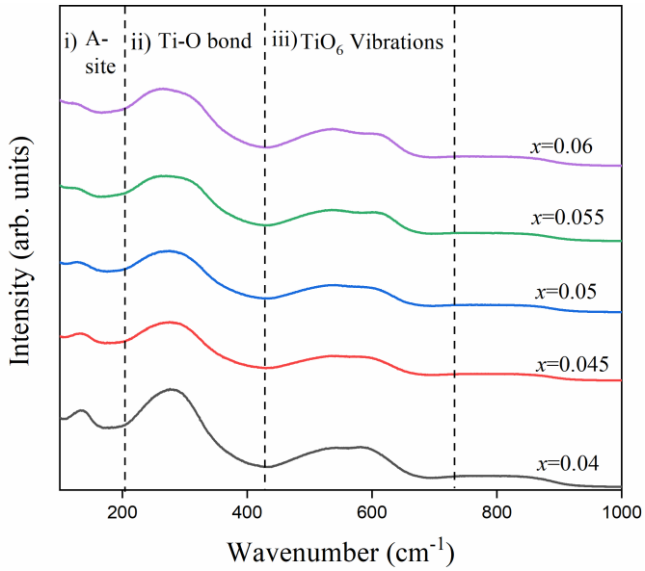

Fig. 5.2 Raman spectrum of (1–x) BNT-xBT (x = 0.040, 0.045, 0.050, 0.055, 0.060).

Fig. 5.2 depicts the Raman spectra of BNT-BT ceramics at room temperature conducted in the range from 100 - 1000 cm^{-1} to verify existence of MPB region. The group theory has predicted four Raman active modes for R3c BNT. The Raman spectra for all solid-solution shows good agreement with the theory. The first two bands has been observed at 130 cm^{-1} and 320 cm^{-1} that corresponds to Bi/Na-O and Ti-O_6 cluster vibrations, respectively [73]. The third mode

lies between 400-800 cm^{-1} which is associated with TiO_6 octahedra vibrations. Above 800 cm^{-1}, A1(LO) and E(LO) overlapping bands are described as the high wavenumber region.

The band seems to broadened or splited at A-site for $x > 0.045$ indicate the coexistence of two phases. Also, with BT content, the peak shifts towards high frequency region (blue shift) that indicate the compressive strains, which has also discussed in the XRD section.

5.3 Scanning Electron Microscope (SEM)

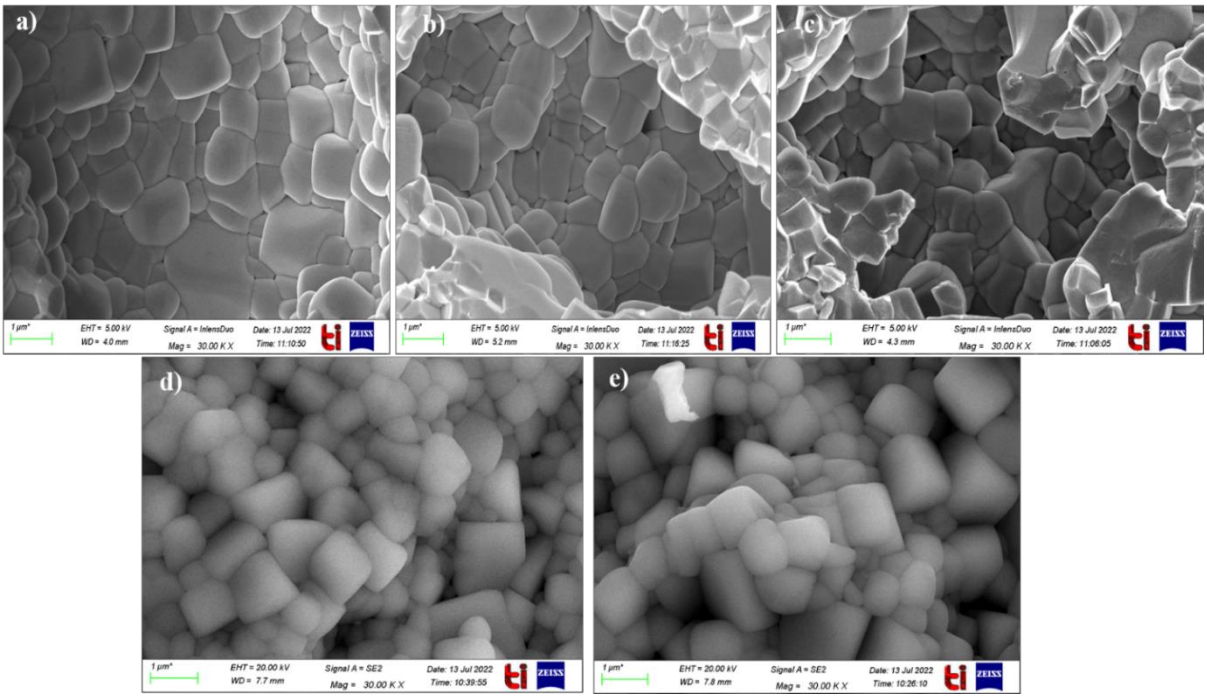

Fig. 5.3 Microstructure of (1–x) $Bi_{0.5}Na_{0.5}TiO_3$-$x$$BaTiO_3$ where x= (0.04, 0.045, 0.05, 0.055, 0.06).

The grain size and its connectivity plays a crucial role to govern the physical properties of ceramics. The highly dense microstructure with low porosity is an ideal for exhibitting good piezo and ferroelectric response. Fig. 5.3 represents the SEM micrographs of fractured BNT-BT ceramics sintered at 1000 °C for 1h. A well dense microstructure has been obtained for all specimens. The average grain size of all ceramics range between 0.5 – 1 μm. However, the addition of BT content leads to decrease in grain size due to the pinning caused by hetro atoms (Ba^{2+}) substituted at A-site that causes compressive strains as already revealed by XRD pattern and Raman spectra.

5.4 Leakage Current Density

Fig. 5.5 illustrates the leakage current density (*J*) of all the specimens with the variation of electric field (E) ranging from -10 kV/cm to 10 kV/cm. The leakage current density increases with applied E and tends to saturate at high field (near 10 kV). Initially the leakage current density increases linearly with E (till 2 kV/cm) for all specimens that indicates the ohmic conduction. This is due to the movement of space charges and generally obtained in low field region. At high field the conduction is governed by lattice distortion, defects, Poole-Frankel effect and hole hopping mechanism. The leakage current density increases with BT content that describes the enhancement of hole hopping mechanism and lattice distortion. Initially, Ba^{2+} occupies interstitial sites of rhombohedral BNT till $x = 0.045$ that contributes to enhance conduction mechanism by the movement of cations. Above $x = 0.045$, the structural distortion of rhombohedral BNT helps to enhance leakage.

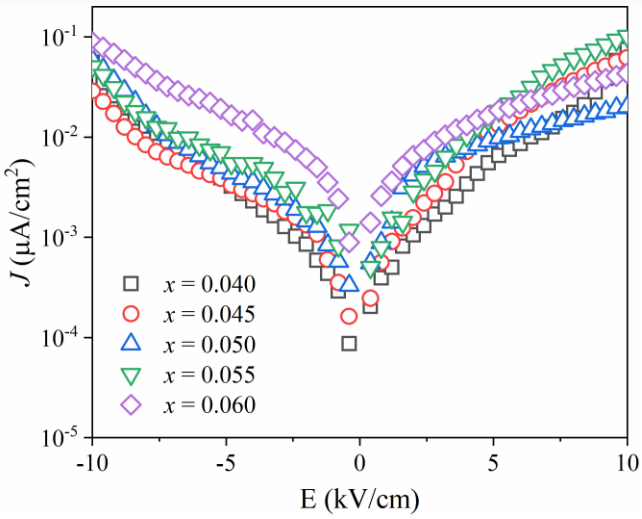

Fig. 5.4 Leakage current density for (1−*x*)BNT–*x*BT (*x* = 0.04, 0.045, 0.05, 0.055, 0.06)

5.5 Dielectric behaviour

Several polarization mechanisms contribute to describe the dielectric properties of specimens, i.e., Dipolar, ionic, electronic, and interfacial polarization. It has already discussed the contribution of space charge carriers overcome with frequency. The frequency dependent dielectric constant (ε_r) of BNT-BT ceramics has shown in Fig. 5.5 (a). It has observed that when frequency increases, the dielectric constant decreases. This dispersion mechanism is completely in accordance to the Maxwell-Wagner polarization theory, which suggest the contribution of grain boundaries in lower frequency region (below 1 kHz), while the dominance of grains at higher frequency range (above 1 kHz). Fig. 5.4 (b) depicts the variation in dielectric

constant (ε_r) of ceramics with BT content at 1 kHz frequency. In this study, it is found that with addition of x content (BT) the value of dielectric constant increases upto x = 0.055 (i.e., $\varepsilon_r \sim$ 1155) and then decreases afterwards. The maximum value of dielectric constant attributes to the higher distortion in the crystal symmetry that activates the ionic charge polarization. This further contributes to enhance the ferroelectric and piezoelectric properties of the specimens.

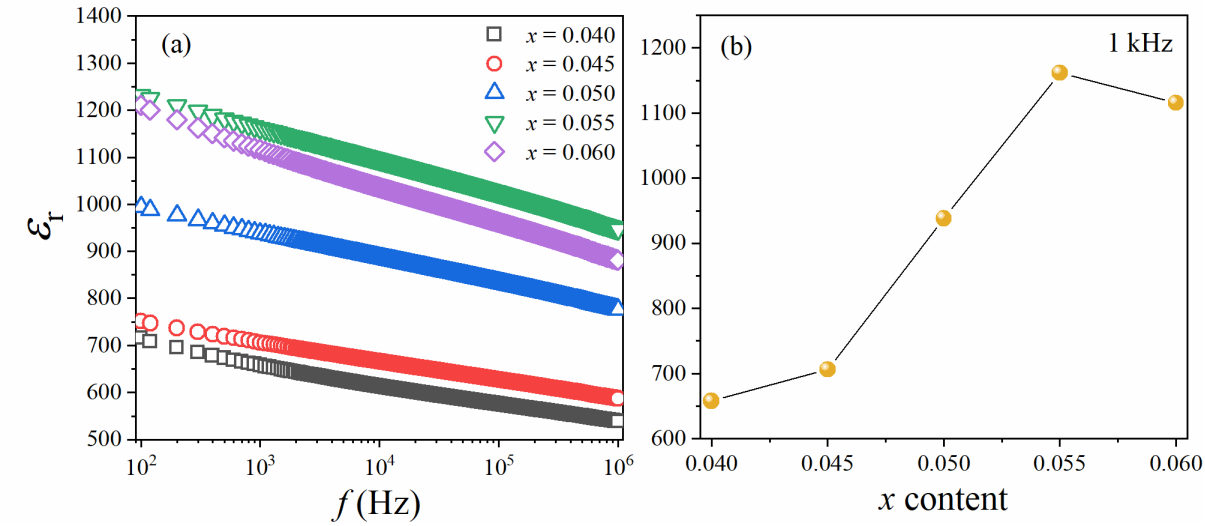

Fig. 5.5 (a) Frequency dependent dielectric constants of (1–x) BNT- xBT with (x = 0.04, 0.045, 0.05, 0.055, 0.06). (b) Dielectric constant variation with the increasing BT content at 1 kHz.

5.6 P-E hysteresis loop

Fig. 5.6 illustrates the P-E hysteresis loop of BNT-BT ceramics at room temperature. All specimens exhibit good hysteresis loops that reflect their good ferroelectric behavior. The graph confirms the detailed dependence of remnant polarization (P_r) and coercive field (E_c) on different composition. It is found that values of remanent polarization for each composition in solid solution is comparable. However, 0.945BNT-0.055BT solid solution exhibits high remanent polarization of 35.6 μC/cm^2 than rest of the specimens. On the other hand, when x = 0.06 the coercive field reaches to 28.6 kV/cm which is less than reported value [74]. It is easier to pole the ceramics with a low coercive field. But for good piezoelectric properties the remanent polarization over coercive field should be large that is pointing towards x = 0.055 specimen.

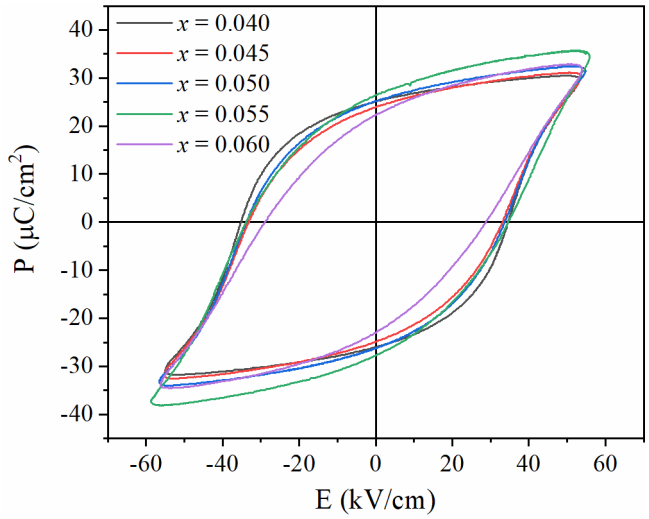

Fig. 5.6 P-E hysteresis loop of (1–*x*)BNT-*x*BT with *x* = (0.04, 0.045, 0.05, 0.055, 0.06).

5.7 Piezoelectric Properties

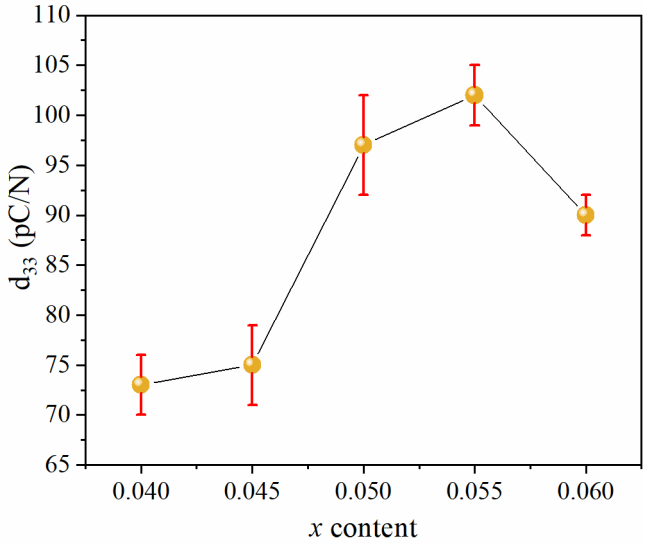

Fig. 5.7 Piezoelectric coefficient d_{33} as a function of x for (1–x) $Bi_{0.5}Na_{0.5}TiO_3$-x$BaTiO_3$.

The presence of several domain states in the MPB solid solution is crucial for good piezoelectric response. Fig. 5.7 shows the variation in piezoelectric coefficient (d_{33}) for all BNT-BT ceramics. Prior to the d_{33} measurements, the samples were corona poled at 10 kV for 2 min by maintaining the specimen to needle separation of 20 mm. It is found that d_{33} increases with BT content till its 5.5% composition in solid solution and then decreases subsequently. The maximum value of d_{33} inside MPB region corresponds to the maximum distortion in the

crystal symmetry. The maximum d_{33} attained is 105 pC/N for 0.945BNT-0.055BT specimen, which is very close to the reported value [59].

Chapter 6
Conclusion & Future Scope

6.1 Conclusion

The solid solution of (1-*x*)BNT-*x*BT was successfully synthesized by the sol-gel method followed by conventional sintering at 1000°C for 1h. The XRD pattern reveals the pure perovskite phase since no impurity peaks were observed. In x = 0.05-0.06 range, the splitting of the intensity peak has confirmed the coexistence of both rhombohedral and tetragonal phase. According to Raman investigation, solid-solution of BNT-BT distorted by BT undergoes structural transformations from rhombohedral to tetragonal phase structure. The SEM micrographs demonstrate the dense microstructure of all solid solutions. The dielectric constant measures the storage capability of all specimens. The BT content enhances the dielectric constant till x = 0.055 and decreases afterwards. The maximum value of dielectric constant for 0.945BNT-0.055BT (ε_r =1155 at 1kHz frequency) indicates the maximum distortion in the crystal symmetry. Further, all specimens exhibit good hysteresis P-E loop. The maximum remanent polarization over coercive field (E_c = 28.6 kV/cm) has been exhibited by x = 0.055 which make it suitable for possessing high piezoelectric coefficient which has further confirmed by d_{33} measurements after corona poling. The maximum d_{33} obtained was 105 pC/N for x = 0.055.

6.2. Future Scope

1. Solid solution of BNT with different lead-free ceramics can be further explained.
2. Piezoelectricity possesses huge amount of application in energy harvesters and piezoelectric generators.

REFERENCES

[1] E. A. Mclaren and R. Giordano, “Ceramics overview : classification by microstructure and processing methods,” vol. 4, no. 3.

[2] “Introduction to Ceramics 1,” pp. 3–4, 2012, doi: 10.1007/978-4-431-54108-0.

[3] M. Stratmann and J. M. Herbert, “Characterization of Materials,” pp. 698–699, 1992.

[4] D. Eliche-quesada and L. Pérez-villarejo, “We are IntechOpen , the world ’ s leading publisher of Open Access books Built by scientists , for scientists TOP 1 % Introduction to Ceramic Materials :,” pp. 0–5.

[5] K. H. Lam, C. L. Sun, K. W. Kwok, and H. L. W. Chan, “Piezoelectric dispenser based on a piezoelectric-metal-cavity actuator,” *Rev. Sci. Instrum.*, vol. 80, no. 7, pp. 1–4, 2009, doi: 10.1063/1.3187220.

[6] R. W. Whatmore, “Piezoelectric and Pyroelectric Materials and Their Applications,” 1991.

[7] F. Reading, “Pacs : 71.18.,” no. 1976, pp. 192–201, 2003.

[8] Y. W. Chung and S. M. Haile, “Introduction to materials science and engineering,” *Phys. Today*, vol. 61, no. 9, pp. 66–68, 2008, doi: 10.1063/1.2982126.

[9] T. E. Problem *et al.*, “Chapter 1: Introduction,” *Microbiology*, no. Musher 2005, pp. 1–74, 2007.

[10] V. Raghavan, *Materials Science and Engineering : a First Course*. Prentice-Hall of India Pvt.Ltd, 2011.

[11] J. Fousek, “Joseph Valasek and the Discovery of Ferroelectricity,” 1847.

[12] O. Access, “We are IntechOpen , the world ’ s leading publisher of Open Access books Built by scientists , for scientists TOP 1 % Based Ceramics and Their.”

[13] S. M. Said, M. F. M. Sabri, F. Salleh, and K. Lumpur, *Ferroelectrics and Their Applications*. Elsevier Ltd., 2017.

[14] “Ferroelectric and Antiferroelectric Liquid,” pp. 1–20, 1974.

[15] D. Brewster, W. Thomson, and W. Voigt, “Pyroelectricity 4,” 2020, doi: 10.1016/B978-0-12-818835-4.00004-3.

[16] P. Ashim and K. Bain, *Bain, Ashim Kumar; Chand, Prem (2017). Ferroelectrics (Principles and Applications)10.1002/9783527805310, doi:10.1002/9783527805310*.

[17] M. Materials, S. Mishra, L. Unnikrishnan, S. K. Nayak, and S. Mohanty, “Advances in Piezoelectric Polymer Composites for Energy Harvesting Advances in Piezoelectric Polymer Composites for Energy Harvesting Applications : A Systematic Review,” no. November, 2018, doi: 10.1002/mame.201800463.

[18] "THE DISCOVERY OF THE PIEZOELECTRIC EFFECT," pp. 15–64, 1880.

[19] W. T. Testing, "Experimental Aeroelastic Investigation using Piezoelectric Transducers in Experimental Aeroelastic Investigation using Piezoelectric Transducers in Wind Tunnel Testing," no. March 2022, 2021, doi: 10.1007/s40799-021-00529-2.

[20] I. Nski, "Fundamentals of Piezoelectricity."

[21] H. Wei *et al.*, "and devices," no. c, pp. 12446–12467, 2018, doi: 10.1039/c8tc04515a.

[22] B. Tiwari, T. Babu, and R. N. P. Choudhary, "Materials Today : Proceedings Piezoelectric lead zirconate titanate as an energy material : A review study," *Mater. Today Proc.*, vol. 43, pp. 407–412, 2021, doi: 10.1016/j.matpr.2020.11.692.

[23] S. C. L. Koh and C. Energy, "Are lead-free piezoelectrics more environmentally friendly ?," vol. 7, no. 1, pp. 1–7, 2017, doi: 10.1557/mrc.2017.10.

[24] N. D. Quan, L. H. Bac, D. Van Thiet, V. N. Hung, and D. D. Dung, "Piezoelectric Materials," vol. 2014, pp. 1–14, 2014.

[25] H. Kabra, H. A. Deore, and P. Patil, "Review on Advanced Piezoelectric Materials," vol. 6, no. 4, pp. 9–12, 2019.

[26] S. Pradhan and G. S. Roy,"Study the Crystal Structure and Phase Transition of $BaTiO_3$ – A Pervoskite," vol. 5, no. 3, pp. 63–67, 2013.

[27] S. E. E. Profile and S. E. E. Profile, "History and Challenges of Barium Titanate : Part I History and Challenges of Barium Titanate : Part I," no. June 2014, 2008, doi: 10.2298/SOS0802155V.

[28] M. A and C. R, "Development and Application of Piezoelectric Materials for Ultrasound Generation and Detection. Ultrasound.," *Ultrasound*, vol. 19, no. 4, pp. 187–196, 2011.

[29] R. Society, "WHO KNEW PIEZOELECTRICITY ? RUTHERFORD AND LANGEVIN ON SUBMARINE DETECTION AND THE INVENTION OF SONAR," vol. 66, no. 2, pp. 141–157, 2016.

[30] B. Jaffe, R. S. Roth, and S. Marzullo, "Ceramics," vol. 809, pp. 10–12, 1954, doi: 10.1063/1.1721741.

[31] R. N. Perumal and V. Athikesavan, "Investigations on electrical and energy storage behaviour of PZN-PT , PMN-PT , PZN – PMN-PT piezoelectric solid solutions," *J. Mater. Sci. Mater. Electron.*, vol. 0, no. 0, p. 0, 2018, doi: 10.1007/s10854-018-0361.

[32] E. Kazuhiko, N. Keiichiro, and M. Keisuke, "PMN-PT and PIN-PMN-PT Piezoelectric Single Crystals with Stable Properties," vol. 27, no. 27, pp. 57–61, 2022.

[33] M. Boldyrev, "Lead: properties, history, and applications," *WikiJournal Sci.*, vol. 1, no. 2, pp. 1–23, 2018, doi: 10.15347/wjs/2018.007.

[34] M. B. Rabinowitz, G. W. Wetherill, J. D. Kopple, M. B. Rabinowrrz, G. W. Wetherill,

and J. D. Kopple, “Kinetic analysis of lead metabolism in healthy humans . Kinetic Analysis of Lead Metabolism in Healthy Humans,” vol. 58, no. 2, pp. 260–270, 1976.

[35] P. K. Panda and B. Sahoo, “PZT to Lead Free Piezo Ceramics : A Review PZT to Lead Free Piezo Ceramics : A Review,” vol. 0193, no. October, 2017, doi: 10.1080/00150193.2015.997146.

[36] W. Van Beveren, “Lead-free piezoceramics,” vol. 432, no. November, pp. 2–5, 2004, doi: 10.1038/nature03008.1.

[37] B. org/10. 1080/00150193. 2015. 1011020. Tio *et al.*, “Dielectric properties of some low-lead or lead-free perovskite-derived,” vol. 26, pp. 3037–3041, 2006, doi: 10.1016/j.jeurceramsoc.2006.02.024.

[38] Y. Hiruma, H. Nagata, T. Takenaka, and S. Member, “Phase-Transition Temperatures and Piezoelectric Properties of ($Bi_{1/2}Na_{1/2}$)TiO_3 -,” vol. 54, no. 12, pp. 2493–2499, 2007.

[39] M. House, I. P. Pronin, P. P. Syrnikov, V. A. Isupov, and V. M. Egorov, “Peculiarities of phase transitions in sodium- bismuth titanate,” no. October 2012, pp. 1–4.

[40] Y. Hiruma, H. Nagata, and T. Takenaka, “Depolarization temperature and piezoelectric properties lead-free piezoelectric ceramics,” vol. 35, pp. 117–120, 2009, doi: 10.1016/j.ceramint.2007.10.023.

[41] Y. Hiruma, H. Nagata, T. Takenaka, Y. Hiruma, H. Nagata, and T. Takenaka, “Thermal depoling process and piezoelectric properties of bismuth sodium titanate ceramics,” vol. 084112, no. 2009, pp. 0–8, 2015, doi: 10.1063/1.3115409.

[42] Y. S. Sung *et al.*, “Effects of Na nonstoichiometry in ($Bi_{0.5}Na_{0.5+x}$)TiO_3 ceramics,” vol. 022901, no. 2010, pp. 2–5, 2014, doi: 10.1063/1.3275704.

[43] P. Igor and R. A. Castro, “Relaxor Properties of Single Crystals,” no. November, pp. 2–5, 2016, doi: 10.1134/S1063785014040245.

[44] K. A. Razak, W. C. Song, and C. Y. Ng, “Combustion Method,” *Procedia Chem.*, vol. 19, pp. 816–821, 2016, doi: 10.1016/j.proche.2016.03.107.

[45] S. Pattipaka, M. Peddigari, and P. Dobbidi, “Effect of Ce on structural and dielectric properties of lead-free ($Bi_{0.5}Na_{0.5}$)TiO_3 ceramics,” no. xxxx, 2017, doi: 10.1016/j.ceramint.2017.05.185.

[46] N. Tio, “Effect of Hf and Li on the structure and electrical properties,” *J. Mater. Sci. Mater. Electron.*, vol. 0, no. 0, p. 0, 2017, doi: 10.1007/s10854-017-7616-9.

[47] B. Na and T. Ceramics, “Processing and Electromechanical Properties of,” vol. 58, pp. 2954–2958, 1997.

[48] Y. Guo, H. Fan, C. Long, J. Shi, L. Yang, and S. Lei, “Electromechanical and electrical properties of,” *J. Alloys Compd.*, 2014, doi: 10.1016/j.jallcom.2014.04.038.

[49] N. Tio, “Effects of Nb^{5+} doping on sintering and electrical properties,” vol. 3, pp. 1140–1143, 2009, doi: 10.1007/s10854-008-9840-9.

[50] O. Paper, V. Pal, O. P. Thakur, and R. K. Dwivedi, “Effect of co-substitution of La / Li on structure , microstructure , dielectric,” vol. 89, no. February, pp. 123–130, 2015, doi: 10.1007/s12648-014-0523-5.

[51] B. Sciencc, “LEAD-FREE PIEZOELECTRIC CERAMICS BASED ON $(Bi_{1/2}Na_{1/2})TiO_3$-$NaNbO_3$ Tadashi Takenaka, Takeo Okuda and Koichi Takegahara,” vol. 03, pp. 175–178, 1997.

[52] B. Chu, D. Chen, G. Li, and Q. Yin, “Electrical properties of $Na_{1/2}$ $Bi_{1/2}TiO_3$ – $BaTiO_3$ ceramics,” vol. 22, pp. 2115–2121, 2002.

[53] N. Bi, “Materials research,” pp. 3–8, 1997.

[54] H. Search, C. Journals, A. Contact, and M. Iopscience, “($Bi_{1/2}Na_{1/2}$)TiO_3-$BaTiO_3$ System for Lead-Free Piezoelectric Ceramics,” vol. 2236.

[55] W. Jo, K. T. P. Seifert, E. Anton, and T. Granzow, “Perspective on the Development of Lead-free Piezoceramics,” vol. 1177, pp. 1153–1177, 2009, doi: 10.1111/j.1551-2916.2009.03061.x.

[56] T. Mei, Q. Dai, W. Zheng, and T. Chen, “Strain properties and piezoelectric constant of lead-free barium titanate ceramics,” *Mater. Res. Express*, vol. 6, no. 10, 2019, doi: 10.1088/2053-1591/ab34b1.

[57] Y. Hiruma, R. Aoyagi, H. Nagata, and T. Takenaka, “Ferroelectric and piezoelectric properties of $(Bi_{1/2}K_{1/2})TiO_3$ ceramics,” *Japanese J. Appl. Physics, Part 1 Regul. Pap. Short Notes Rev. Pap.*, vol. 44, no. 7 A, pp. 5040–5044, 2005, doi: 10.1143/JJAP.44.5040.

[58] M. Munir *et al.*, “synthesized by sol – gel method,” *J. Sol-Gel Sci. Technol.*, 2019, doi: 10.1007/s10971-018-04913-0.

[59] Y. Liu, W. Ren, J. Zhao, L. Wang, P. Shi, and Z. Ye, “Effect of sintering temperature on structural and electrical properties of lead-free BNT – BT piezoelectric thick fi lms,” *Ceram. Int.*, pp. 1–6, 2015, doi: 10.1016/j.ceramint.2015.03.255.

[60] F. Guo *et al.*, “lead-free piezoelectric ceramics Morphotropic phase boundary and electric properties in,” vol. 124113, no. 2012, pp. 2010–2015, 2014, doi: 10.1063/1.4730770.

[61] S. Li, L. Chen, X. Ning, M. Guo, and M. Zhang, “Preparation from hydrothermally synthesized precursor powders,” *Ceram. Int.*, vol. 41, no. 1, pp. 195–204, 2015, doi: 10.1016/j.ceramint.2014.08.058.

[62] E. Properties *et al.*, “Qi Wang, Jun Chen , Longlong Fan, Huidong Song, Wei Gao,Yangchun Rong, Laijun Liu, Liang Fang, and Xianran Xing ,” vol. 3797, pp. 3793–

3797, 2013, doi: 10.1111/jace.12588.

[63] S. Zhang, F. Yan, and B. Yang, “x Bi $(Zn_{0.5}Ti_{0.5})O_3$ lead-free piezoceramics Morphotropic phase boundary and electrical properties in,” vol. 114110, no. 2010, pp. 1–5, 2013, doi: 10.1063/1.3431387.

[64] L. Piezoceramics *et al.*, “Qi Wang, Jun Chen, Longlong Fan, Laijun Liu, Liang Fang, and Xianran Xing ,” vol. 1175, pp. 1171–1175, 2013, doi: 10.1111/jace.12147.

[65] Y. Hiruma, Y. Imai, Y. Watanabe, H. Nagata, and T. Takenaka, “Large electrostrain near the phase transition temperature of $(Bi_{0.5}Na_{0.5})TiO_3 – SrTiO_3$ ferroelectric ceramics Large electrostrain near the phase transition temperature of,” vol. 262904, no. 2008, pp. 2–5, 2014, doi: 10.1063/1.2955533.

[66] S. Response, B. Na, À. Tio, B. Al, and T. O. Ceramics, “Wangfeng Bai, Yanlong Bian, Jigong Hao, Bo Shen, and Jiwei Zhai,” vol. 252, pp. 246–252, 2013, doi: 10.1111/jace.12039.

[67] P. Piezoelectric, E. Strain, and L. Ceramics, “Feng Li, Ruzhong Zuo, Donggeng Zheng, and Longtu Li ,” vol. 8, pp. 1–8, 2014, doi: 10.1111/jace.13363.

[68] B. Cullity, *Elements of X-Ray Diffraction*.

[69] H. Seiler, “Secondary electron emission in the scanning electron microscope Secondary electron emission in the scanning electron microscope ,” vol. 1, 1983, doi: 10.1063/1.332840.

[70] P. Taylor, C. Eisenschmidt, H. T. Langhammer, and R. Steinhausen, “Ferroelectrics Tetragonal-Orthorhombic Phase Transition in Barium Titanate via Monoclinic M C Type Symmetry,” no. October 2012, pp. 37–41, doi: 10.1080/00150193.2012.707894.

[71] V. A. Online, M. V. R. Reddy, and N. Kalarikkal, “RSC Advances,” 2016, doi: 10.1039/C5RA18018J.

[72] F. Ceramics *et al.*, “Accepted Manuscript,” 2014, doi: 10.1016/j.jallcom.2014.08.161.

[73] N. Na *et al.*, “Structural, optical, and electrical properties of Nd-doped $Na_{0.5}Bi_{0.5}TiO_3$,” *Mater. Chem. Phys.*, vol. 134, no. 2–3, pp. 829–833, 2012, doi: 10.1016/j.matchemphys.2012.03.076.

[74] B. Na *et al.*, “Intrinsic and extrinsic electric response in,” *Ferroelectrics*, vol. 547, no. 1, pp. 156–163, 2019, doi: 10.1080/00150193.2019.1592495.